Archives of Hydro-Engineering and Environmental Mechanics
Vol. 50 (2003), No. 3, pp. 165–192

Lagrangian-Eulerian Approach to Modelling of Wave Transformation and Flow Velocity in the Swash Zone and its Seaward Vicinity

Jarosław Kapiński

Institute of Hydro-Engineering of the Polish Academy of Sciences
ul. Kościerska 7, 80-953 Gdańsk, Poland, e-mail: kapinski@ibwpan.gda.pl

(Received April 04, 2002; revised October 02, 2003)

Abstract

One-dimensional long waves approaching a beach face are investigated herein. In particular, flow velocity distribution, wave profile transformation and extreme positions of a water uprush-backwash are analysed. For simplicity, non-dissipative waves, waves influenced by linear or quadratic bottom friction, as well as bore-like breaking waves are considered separately. Bore formation and propagation in a shoaling water is modelled by geometrical limitation of a local slope of the wave front. Analysed phenomena are described using the shallow-water wave theory, although in this paper application of the model has been restricted to the swash zone and its seaward vicinity. Governing equations are expressed in hybrid Lagrangian-Eulerian co-ordinates. The Lagrangian approach gives a precise mathematical description of both an orbital motion and the moving position of a water tongue on a beach slope. The Eulerian contribution to the model enables easy comparison of results of wave and water motion by method of conducting of measurements. Moreover, the hybrid description affords the possibility of simple prediction of mean water flow caused by propagating waves. The following description also presents results of numerical computations especially concerning wave run-up height, flow and orbital velocities and water surface transformation. For simplified bathymetric conditions some analytical solutions are also presented.

Key words: wave run-up, swash zone, mass transport, Lagrangian approach, wave breaking

Notation

- a – acceleration at cross-section x,
- a^{ξ} – acceleration at cross-section x^{ξ}, i.e. water particle acceleration,
- c – shallow-water wave celerity,
- D_b^{ξ} – force, divided per unit surface, causing loss of momentum due to wave breaking,

f – bottom friction coefficient,
f_V – bottom friction coefficient after Voltzinger et al (1989),
g – gravitational acceleration,
h – water depth at cross-section x,
h^{ξ} – water depth at cross-section x^{ξ},
H – incident wave height,
H_s – significant wave height,
i – imaginary unit,
Ir – Iribarren number,
J_n – Bessel function of n-th order,
k – wave number,
l – horizontal distance between slope toe and junction of *SWL* with bottom slope,
L – incident wavelength,
Q – water discharge,
R_{back} – wave run-back length,
R_{down} – wave run-down height,
R_{on} – wave run-on length,
R_{up} – wave run-up height,
R_{us} – significant wave run-up height,
S – local surface steepness of wave front at cross-section x,
S^{ξ} – local surface steepness of wave front at cross-section x^{ξ},
S_b^{ξ} – critical surface steepness of wave front,
t – time,
T – wave period,
v – flow velocity at cross-section x,
$\bar{v}$ – time-averaged flow velocity at cross-section x (return flow velocity),
$\overline{v^S}$ – Stokes drift (according to Andrews and McIntyre terminology),
v^{ξ} – velocity at cross-section x^{ξ}, i.e. water particle velocity,
$\overline{v^{\xi}}$ – time-averaged water particle velocity,
v_0^{ξ} – velocity of water tongue tip,
x – position of particle till initial instant $t = 0$, also horizontal co-ordinate,
x^{ξ} – position of particle at time t,
z – vertical co-ordinate,

α – angle of a constant bottom slope,
ζ – water surface elevation at cross-section x,
ζ_0 – water surface elevation at junction of *SWL* with bottom slope, i.e. at $x = 0$,
ζ^{ξ} – water surface elevation at cross-section x^{ξ},
ξ – displacement of particle,
$\bar{\xi}$ – time-averaged water particle displacement,
ξ_{max} – amplitude of particle displacement,
ξ_0 – displacement of water tongue tip,
ρ – water density,
τ^{ξ} – bottom shear stress at cross-section x^{ξ},
τ_*^{ξ} – total force, divided per unit surface, causing loss of momentum at cross-section x^{ξ},
ϕ – any hydrodynamical parameter expressed in the Eulerian sense,
ϕ^{ξ} – any hydrodynamical parameter expressed in the Lagrangian sense,
ω – angular frequency.

1. Introduction

A swash zone is a specific section of the coastal area in which the wave motion differs considerably from the rest. Visually it evinces in the oscillatory nature of water uprush-backwash on a beach face. In realistic conditions, i.e. on ocean or sea beaches, irregular and mostly breaking waves are observed. In addition, they are affected by bottom roughness and permeability. Complexity of these phenomena is the reason why the description of water tongue behaviour on a slope is still unsatisfactory. Laboratory and field investigations mainly concentrate on measurements of wave run-up and run-down heights. The results are usually shown as a function of the Iribarren number (Iribarren, Nogales 1949). Less attention is paid to transformation of the water surface, however, it is a determinant of the condition of a wave climbing the slope. The most complicated seems to be analysis of flow velocity within a water tongue. Lack of satisfactory measurements useful for comparison is due to spatial and time variability of the velocity and its direction. Additional impediments arise from a changeable water tongue thickness, contamination with air bubbles and sandy material, as well as successive presence and absence of the water body on the beach face.

Within various shallow-water descriptions, the most frequently developed models are those which use an Eulerian co-ordinate system. Unfortunately, they usually fail in the case of precise modelling of a shoreline motion. Very complex or – on the contrary – quite simplified mathematical assumptions at the intersection

of SWL (Still Water Level) with a beach or numerical algorithms for simulation of an "artificial" water tongue motion often produce computational difficulties. They result in numerical instability or in inaccuracy of unknown magnitude. This problem disappears in models elaborated in a Lagrangian co-ordinate system, for which a landward boundary condition is easy to satisfy. The effect is an exact mathematical description of a time-dependent position of a water tongue tip as well as a velocity pattern within the water tongue. Another advantage of the Lagrangian approach arises from the treatment of a water body as a collection of travelling particles with fixed identities. It provides fully-detailed information on an orbital motion from which the surface of water waves can be computed in an easy and exact manner.

The first Lagrangian description of the swash zone was elaborated by Miche (1944). His model is based on low, sinusoidal waves running up a steep and uniformly sloping beach. He obtained the following solution:

$$v_0' = \frac{1}{\sin\alpha}\frac{\pi H}{2}\sqrt{\frac{g}{\alpha L}}\cos\left(\sqrt{\frac{2\pi g}{L}}t\right), \tag{1}$$

where:

v_0' – velocity of water tongue tip parallel to the beach face,
H – wave height,
L – wavelength,
α – beach slope.

A horizontal component of the velocity v_0^{ξ} can be obtained by a simple multiplication by $\cos\alpha$. Miche showed that for oncoming sinusoidal waves both the movement and the velocity of a water edge can be described with a time-dependent sinusoidal function.

The first comprehensive mathematical description of the shallow-water wave motion in the Lagrangian co-ordinates was made by Shuto (1967, 1968, 1972 and 1978). In 1967 he presented a two-dimensional (in a vertical plane) model for a non-breaking wave propagation and run-up on a beach face. Next, in 1968 Shuto solved the same problem for a three-dimensional case. In 1972 he obtained a solution of a run-up height for standing small-amplitude waves on a beach with a uniform slope:

$$\frac{R_{up}}{H} = \left(J_0^2\left(4\pi\frac{l}{L}\right) + J_1^2\left(4\pi\frac{l}{L}\right)\right)^{-0.5}, \tag{2}$$

where:

R_{up}/H – normalised wave run-up height,

J_n – Bessel function of the n-th order,
l – horizontal length of a slope,
L – wavelength.

Equation (2) is identical with the earlier Keller and Keller's solution (1964) who employed a Eulerian point of view. The same equation was also derived by Kapiński and Kołodko (1996) for the model that is developed in further sections of this paper. In 1978 Shuto and Goto (1978) presented numerical results of a one-dimensional Lagrangian model for prediction of tsunami run-up on non-planar beaches. An improvement of the Shuto's model (1967) was made by Goto (1979). He derived non-linear equations and solved them numerically. Goto compared the obtained results with those of Shuto (1972) and showed that non-linear effects in computations of a run-up height do not exceed 10–20%. Another two-dimensional Lagrangian model was presented by Nishimura and Takewaka (1987). They investigated small amplitude waves sloshing in a rectangular tank with a horizontal bottom and vertical walls and analysed water surface elevations and flow velocities inside the water body. One of the recent models in the Lagrangian co-ordinates was presented by Zelt and Raichlen (1990). They derived and solved numerically depth-averaged equations of long wave propagation and run-up on a plane and impermeable beach. Next, Zelt (1991) included dissipative terms due to wave breaking and bottom friction quadratic with the flow velocity. Wave breaking and bore propagation was modelled adopting artificial viscosity technique (von Neuman and Richtmyer 1950) and as a breaking criterion a maximum velocity gradient was adopted. Zelt studied water surface elevations and run-up heights of a solitary wave while flow velocities were not analysed there.

A new idea in modelling of a wave and wave-induced water motion was introduced by Andrews and McIntyre (1978) and called a Generalised Lagrangian-mean (*GLM*) method. A valuable discussion on it can also be found in McIntyre (1980) and Dingemans (1997). A basic advantage of the method is a precise identification of mean water flow in an oscillatory wave field. Thus, the influence of wave motion on mean flows can be investigated. It is conducted by means of a hybrid Lagrangian-Eulerian approach, in which, considerably simplifying explanation, mean values following an orbital motion (i.e. Lagrangian means) and mean values at fixed cross-sections (i.e. Eulerian means) are taken into account. The difference between Lagrangian and Eulerian mean velocity is called by Andrews and McIntyre (1978) a Stokes drift.

The mathematical model used in this paper was described by Kapiński and Kołodko (1996) and Kapiński (1998). In the first work the formulation of the model and brief discussion on a shallow-water wave motion in mixed Lagrangian-Eulerian co-ordinates was given. It was pointed out that the model is capable of predicting both wave run-up on a beach face and an orbital motion of particles in a shallow water area. The second work contains more detailed analysis

including bore-like breaking waves and waves influenced by the bottom friction that is linear with flow velocity ($\tau \sim v$). In this paper some new elements, e.g. quadratic bottom friction ($\tau \sim v^2$), are implemented. Additionally, new investigations on orbital (Lagrangian) and flow (Eulerian) velocities are presented. This concerns both the swash zone and its seaward vicinity.

2. General Description of the Model

A simple shallow-water model in the hybrid Lagrangian-Eulerian co-ordinates is presented herein. Description of a wave motion is based on depth-averaged momentum and mass conservation equations, where inviscid and small-amplitude waves are considered. Thus, uniform velocity in vertical (both Lagrangian and Eulerian one) and a hydrostatic pressure are assumed. For convenience, an impermeable and fixed bottom is assumed, although an implementation of a bottom profile in compliance with shear stress seems to be feasible. Additionally, the influence of different external factors such as wind force or longshore currents has been neglected.

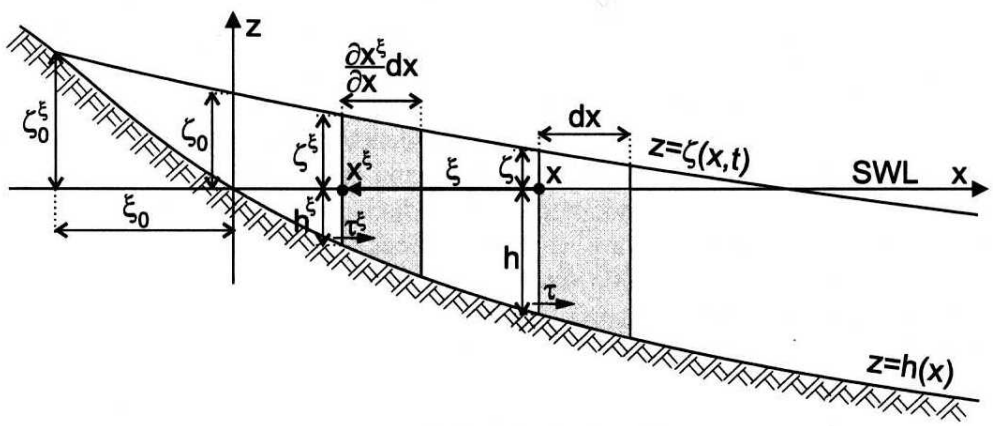

Fig. 1. Definition sketch of model

A definition sketch of the model is shown in Fig. 1. A horizontal axis of the co-ordinate system is located on Still Water Level (*SWL*) and is directed offshore. A vertical axis intersects the horizontal one at the point of junction of *SWL* with a slope. A selected water particle to the initial instant, $t = 0$, occupies position x. Because of wave motion the particle commence excursion and its displacement is denoted as $\xi = \xi(x,t)$. Thus, an instantaneous particle position at time t is given by $x^\xi = x + \xi$[1]. Water level elevation and water depth at cross-section x, that is fixed in time, are denoted as ζ and h, respectively. Similarly, the elevation

[1] Superscript ξ is used to mark parameters performing at cross-section $x + \xi$, while for parameters performing at cross-section x no indication is given.

and depth at cross-section x^ξ, moving together with the particle, are denoted as ζ^ξ and h^ξ. In addition, signs of parameters h and h^ξ are taken inversely, i.e. they have positive values below *SWL*. Horizontal movement of a water tongue tip ξ_0 is represented by displacements of a particle occupying position $x = 0$ at the initial instant. Its maximum onshore position on a slope is given as run-on length R_{on}. Maximum vertical position of a water tongue on the slope (run-up height) is described as R_{up}. In addition, instantaneous water elevation at a fixed cross-section $x = 0$ is denoted in Fig. 1 as ζ_0.
Some of the above considerations can be summarised as follows:

$$\begin{aligned} &\xi = \xi(x,t), \quad x^\xi = x^\xi(x,t) = x + \xi(x,t), \quad \xi_0 = \xi(x=0,t), \\ &\zeta = \zeta(x,t), \quad \zeta^\xi = \zeta\left(x^\xi,t\right) = \zeta(x+\xi,t), \quad \zeta_0 = \zeta(x=0,t), \\ &h = h(x), \quad h^\xi = h\left(x^\xi\right) = h(x+\xi). \end{aligned} \tag{3}$$

It is worth mentioning here that such parameters as displacement of a particle ξ, its instantaneous position x^ξ and an elevation of a water surface ζ^ξ corresponding to this position have a Lagrangian meaning, while water elevation ζ at motionless cross-section x is a typical variable expressed in a Eulerian sense.

Depth-averaged momentum and mass conservation equations are expressed in the Lagrangian sense as follows (Kapiński and Kołodko 1996):

$$\rho\left(h^\xi + \zeta^\xi\right)\frac{\partial x^\xi}{\partial x}dx\frac{\partial^2\xi}{\partial t^2} + \rho g\left(h^\xi + \zeta^\xi\right)\frac{\partial \zeta^\xi}{\partial x}dx = \tau_*^\xi\frac{\partial x^\xi}{\partial x}dx, \tag{4}$$

$$\rho h dx = \rho\left(h^\xi + \zeta^\xi\right)\frac{\partial x^\xi}{\partial x}dx, \tag{5}$$

where:

$$\frac{\partial x^\xi}{\partial x} = 1 + \frac{\partial \xi}{\partial x},$$

g – gravitational acceleration,
ρ – water density.

The term on the right-hand side of Eq. (4) represents all external forces acting at cross-section x^ξ that are responsible for the loss of a wave momentum. Parameter τ_*^ξ is the sum of bottom friction τ^ξ and a force, divided per unit surface, arising from a wave breaking D_b^ξ:

$$\tau_*^\xi = \tau^\xi + D_b^\xi. \tag{6}$$

More detailed discussion on the parameter τ_*^ξ will be given in following sections and until then let it be assumed as a known function.

From Equation (5) we have:

$$\zeta^{\xi} = h/\frac{\partial x^{\xi}}{\partial x} - h^{\xi}. \tag{7}$$

Now, substitution of ζ^{ξ} and its derivative $\frac{\partial \zeta^{\xi}}{\partial x}$ to Eq. (4) yields:

$$\frac{\partial^2 (h\xi)}{\partial t^2} = gh\frac{\frac{\partial}{\partial x}\left(h^{\xi} - h/\frac{\partial x^{\xi}}{\partial x}\right)}{\frac{\partial x^{\xi}}{\partial x}} + \tau_*^{\xi}\rho/\frac{\partial x^{\xi}}{\partial x}. \tag{8}$$

Equation (8) is difficult, if ever possible, to solve and therefore some simplifications are introduced here. First assumption, $\left|\frac{\partial^2 h}{\partial x^2}\right| \ll 1$, reduces the shape of a bottom to that of a small curvature, however, points with bends are acceptable here. The second one, $\left|\frac{\partial \xi}{\partial x}\right| \ll 1$, imposes small gradients of particle displacements. In the light of these conditions the following approximate formulas are valid:

$$h^{\xi} = h + \xi\frac{\partial h}{\partial x}, \quad 1 - \frac{\partial \xi}{\partial x} = \frac{1}{1 + \frac{\partial \xi}{\partial x}}, \tag{9}$$

which are then inserted into Eqs. (7) and (8).

Now, after assessment and neglecting of negligible terms, Eqs. (8) and (7), may be rewritten as follows:

$$\frac{\partial^2 (h\xi)}{\partial t^2} = gh\frac{\partial^2 (h\xi)}{\partial x^2} + \frac{\tau_*^{\xi}}{\rho}, \tag{10}$$

$$\zeta^{\xi} = -\frac{\partial (h\xi)}{\partial x}. \tag{11}$$

Equation (10) describes depth-averaged displacement of a particle ξ, while from Eq. (11) elevation of a water surface ζ^{ξ} in position $x^{\xi} = x + \xi$ can be calculated. The water elevation ζ at a fixed cross-section x, i.e. in the Eulerian sense, can be assessed for every cross-section from a Taylor series expansion:

$$\zeta \approx \zeta^{\xi} - \xi\frac{\partial \zeta^{\xi}}{\partial x}, \tag{12}$$

or computed numerically where neighbouring elevations ζ^{ξ} are taken into account.

Combining Eqs. (10) and (11) we have another equation that is equivalent to the wave equation expressed in the Eulerian sense:

$$\frac{\partial^2 \zeta^{\xi}}{\partial t^2} = \frac{\partial \left(gh \frac{\partial \zeta^{\xi}}{\partial x} \right)}{\partial x} - \frac{\frac{\partial \tau_*^{\xi}}{\partial x}}{\rho}, \tag{13}$$

where the term gh denotes the square of a shallow-water wave celerity c^2.

3. Non-dissipative Model

3.1. Movable Boundary Description

As a first approach to the analysis of a wave motion, forces causing loss of momentum are dropped in the considerations, $\tau_*^{\xi} = 0$. Then Eqs. (10) and (13) simplify to the forms:

$$\frac{\partial^2 (h\xi)}{\partial t^2} = gh \frac{\partial^2 (h\xi)}{\partial x^2}, \tag{14}$$

$$\frac{\partial^2 \zeta^{\xi}}{\partial t^2} = \frac{\partial \left(gh \frac{\partial \zeta^{\xi}}{\partial x} \right)}{\partial x}. \tag{15}$$

It is easy to show that there are no difficulties with a description of a landward movable boundary, especially for the rigid bottom assumed in the model for which depth h is not a function of time t. A particle which occupied the peripheral position on a slope up till the arrival of the first wave, i.e. $x = 0$ for which the depth $h = 0$, will always represent the edge of a floating water tongue. Inserting $h = h_0 = 0$ into Eqs. (14) and (11) a complete description of motion of the tongue tip is obtained:

$$\frac{\partial^2 \xi_0}{\partial t^2} = g \left(\xi_0 \frac{\partial^2 h_0}{\partial x^2} + 2 \frac{\partial h_0}{\partial x} \frac{\partial \xi_0}{\partial x} \right), \tag{16}$$

$$\zeta_0^{\xi} = -\xi_0 \frac{\partial h_0}{\partial x}. \tag{17}$$

Extreme values of the parameter ζ_0^{ξ} correspond to the run-up height R_{up} and run-down height R_{down}, and in a similar way, extreme values of ξ_0 – to the run-on length R_{on} and run-back length R_{back}.

3.2. Mass Transport Modelling

So far, a pure Lagrangian description of a wave motion was used whereas in the following analysis a hybrid Lagrangian-Eulerian approach is involved. First, a mean Lagrangian displacement and velocity are calculated. Next, a mean velocity in the Eulerian sense is derived and finally the difference between both

velocities is analysed. Probably it is the simplest possible application of the *GLM* theory elaborated by Andrews and McIntyre (1978) to the modelling of coastal hydrodynamics.

During propagation of a linear progressive wave, particles move in closed elliptical paths. Thus, a horizontal particle displacement can be described by the following equation:

$$\xi = \xi_{\max} \cos(kx + \omega t), \tag{18}$$

where in front of the term ωt appears a *plus* sign because of the opposite direction of wave propagation in relation to the x-axis (cf. Fig. 1).

For a depth-averaged flow, the ratio of lengths of the ellipse semiaxes is as follows:

$$\frac{\xi_{\max}}{H/2} = \frac{1}{kh}. \tag{19}$$

This corresponds to the quotient of the maximum horizontal to maximum vertical particle displacement in the model. Substitution of Eq. 19 into Eq. 18 yields:

$$\xi = \frac{H}{2kh} \cos(kx + \omega t). \tag{20}$$

Thus, a particle velocity is described by the following equation:

$$v^{\xi} = \frac{\partial \xi}{\partial t} = -\frac{\omega H}{2kh} \sin(kx + \omega t). \tag{21}$$

Now, it can easily be proved that mean values of ξ and v^{ξ} are equal to zero:

$$\overline{\xi} = \frac{1}{T}\int_0^T \xi dt \equiv 0, \quad \overline{v^{\xi}} = \frac{1}{T}\int_0^T v^{\xi} dt \equiv 0, \tag{22}$$

where the overbar denotes time averaging over wave period T.

Any hydrodynamical parameter can be expanded around x^{ξ} in the Taylor series in the following way:

$$\phi = \phi^{\xi} - \xi \frac{\partial \phi^{\xi}}{\partial x} + 0.5\xi^2 \frac{\partial^2 \phi^{\xi}}{\partial x^2} - \ldots, \tag{23}$$

where ϕ and ϕ^{ξ} are certain parameters expressed in Eulerian and Lagrangian co-ordinates, respectively. Thus, for example, a water level elevation and flow velocity at cross-section x take the following forms:

$$\zeta = \zeta^{\xi} - \xi \frac{\partial \zeta^{\xi}}{\partial x} + 0.5\xi^2 \frac{\partial^2 \zeta^{\xi}}{\partial x^2} - \ldots, \tag{24}$$

$$v = v^{\xi} - \xi \frac{\partial v^{\xi}}{\partial x} + 0.5\xi^2 \frac{\partial^2 v^{\xi}}{\partial x^2} - \dots \,. \tag{25}$$

Substitution of Eqs. (20) and (21) into linearized Eq. (25) yields:

$$v = \frac{\omega H}{2kh}\left[-\sin(kx + \omega t) + \frac{H}{2h}\cos^2(kx + \omega t)\right]. \tag{26}$$

After averaging over a wave period T a mean Eulerian velocity, called here a return flow, we obtain:

$$\overline{v} = \frac{1}{T}\int_0^T v dt = \frac{1}{8}\left(\frac{H}{h}\right)^2 c. \tag{27}$$

Using the same way of derivation, it can easily be shown that for standing waves, for which displacements of particles are described by the following equation:

$$\xi = 2\xi_{\max} \cos kx \cos \omega t, \tag{28}$$

mean flow velocity at any cross-section is equal to zero, $\overline{v} = 0$. Moreover, it can be proved that mean water discharge for both progressive and standing waves also amounts to zero, $Q = 0$. These and many other Lagrangian and Eulerian parameters obtained from this analysis are summarised in Table 1. From the above text it can be concluded that no resultant water discharge occurs and thus the mass conservation law is still satisfied. However, non-zeroth mean flow velocity directed offshore (i.e. return flow velocity) is present, cf. Eq. (27). It is the effect of a slight deviation of a modelled wave profile from the sine function.

Andrews and McIntyre (1978) in their work analysed a mean water flow, called by them a Stokes drift, which is the difference between a Lagrangian and Eulerian mean velocity:

$$\overline{v^S} = \overline{v^{\xi}} - \overline{v}. \tag{29}$$

Thus for the linear case presented here, the Stokes drift for long progressive waves in shallow water is described as follows:

$$\overline{v^S} = -\frac{1}{8}\left(\frac{H}{h}\right)^2 c, \tag{30}$$

where Eqs. (22) and (27) were used.

It is worth mentioning here, that the velocity is negative and therefore the drift direction always coincides with a wave propagation (cf. Fig. 1). As is known, Eq. (30) also describes the Stokes' drift for progressive second-order waves derived in

Table 1. Summary of water elevation and velocity for progressive and standing waves

Description	Progressive wave	Standing wave
Particle displacement	$\xi = \frac{H}{2kh} \cos(kx + \omega t)$	$\xi = \frac{H}{2kh} \cos kx \cos \omega t$
Extreme particle displacement	$\xi_{extr} = \pm \frac{H}{2kh}$	
Mean particle displacement	$\bar{\xi} = 0$	
Water elevation	$\zeta = \frac{H}{2} \times \left(\sin(kx + \omega t) - \frac{H}{2h} \cos^2(kx + \omega t) \right)$	$\zeta = H \cos kx \sin \omega t \times \left(1 + \frac{H}{2h} \sin kx \cos \omega t \right)$
Extreme water elevation	$\zeta_{extr} = \pm \frac{H}{2}$	$\zeta_{extr} = \pm H$
Mean water elevation	$\bar{\zeta} = -\frac{H^2}{8h}$	$\bar{\zeta} = 0$
Particle velocity	$v^{\xi} = -\frac{\omega H}{2kh} \sin(kx + \omega t)$	$v^{\xi} = -\frac{\omega H}{2kh} \cos kx \sin \omega t$
Extreme particle velocity	$v^{\xi}_{extr} = \pm \frac{\omega H}{2kh} = \pm \frac{H}{h} \frac{c}{2}$	
Mean particle velocity	$\overline{v^{\xi}} = 0$	
Instant mass transport velocity	$v^{S} = -\frac{\omega H}{2kh} \times \left[-\sin(kx + \omega t) + \frac{H}{2h} \cos^2(kx + \omega t) \right]$	$v^{S} = \frac{\omega H}{2kh} \cos kx \times \sin \omega t \left[1 + \frac{H}{2h} \sin kx \cos \omega t \right]$
Extreme mass transport velocity	$v_{extr} = \pm \frac{\omega H}{2kh} = \pm \frac{H}{h} \frac{c}{2}$	
Mass transport velocity	$\overline{v^{S}} = -\frac{1}{8} \left(\frac{H}{h} \right)^2 c$	$\overline{v^{S}} = 0$
Water discharge	$\overline{Q} = 0$	

Eulerian co-ordinates (e.g. van Rijn 1993). This means that the magnitude of the velocity $\overline{v}$ can be obtained in this model already in the linear approach, despite the Eulerian method where non-linear analysis is necessary. The only difference is that for Lagrangian waves particles draw closed trajectories. Thus resultant water discharge there amounts to zero.

Equation (30) describes the Stokes drift performing at constant water depth. For uneven bottom shapes, when the condition $\left|\frac{\partial^2 h}{\partial x^2}\right| \ll 1$ is satisfied, it can only be computed numerically. Relevant numerical examples are presented in Section 6.

4. Model with Bottom Friction

This paper analyses two simplified formulas taking bottom friction into account. The first formula, taken after Voltzinger et al (1989) and rewritten in Lagrangian co-ordinates,

$$\tau^{\xi} = -f_V \rho h \frac{\partial \xi}{\partial t}, \tag{31}$$

where: f_V – friction coefficient, shows linear dependence of shear stress τ^{ξ} on particle velocity $v^{\xi} = \frac{\partial \xi}{\partial t}$. Validity of the equation is for: $f_V \ll \omega$ (Voltzinger et al 1989).

The second formula describes a bottom friction quadratic with a horizontal particle velocity:

$$\tau^{\xi} = -0.5 f \rho \left|\frac{\partial \xi}{\partial t}\right| \frac{\partial \xi}{\partial t}, \tag{32}$$

and is also rewritten in Lagrangian co-ordinates.

Both equations can be used in the model alternatively, however, for wave simulation the second one requires much more computational time. The relevant numerical example of the wave motion disturbed by bottom friction is shown in Section 6.

5. Model with a Bore-like Breaking Wave

5.1. Adaptation of a Breaking Criterion

Modelling of breaking waves is still one of the most difficult problems to solve among coastal zone phenomena. In the case of gently sloping beaches the analogy to bore propagation is often used. In this model, the bore-like breaking process has also been adopted. It is realised by means of the reduction of excessive steepening of a wave travelling in shoaling water. Then local steepness of water surface S^{ξ} (cf. Fig. 2) cannot exceed some critical value S_b^{ξ} at any point of the wave front. In this way, further growth of wave height towards the shore is avoided.

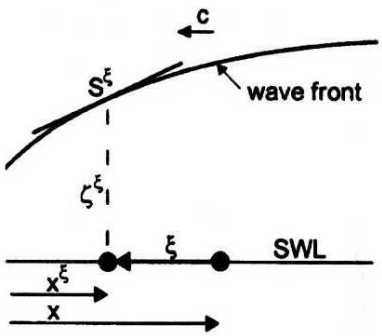

Fig. 2. Sketch of wave front

In general, the parameter S^ξ describes a local surface steepness:

$$S^\xi = \frac{\partial \zeta^\xi}{\partial x^\xi} = \frac{\partial \zeta^\xi}{\partial x} \Big/ \frac{\partial x^\xi}{\partial x}, \tag{33}$$

but its definition in the model has been limited to the wave front, i.e. when both $\xi \leq 0$ and $\zeta^\xi \geq 0$. The magnitude of the parameter S_b^ξ will be assessed in Section 5.2. on the basis of laboratory experiments, hence let it be taken as a constant value. An Eulerian counterpart of S^ξ is a local steepness at cross-section x, $S = \frac{\partial \zeta}{\partial x}$.

If a local steepness S^ξ at any point of a wave front x^ξ is exceeded, it is artificially reduced to the required value S_b^ξ. This means that the dissipative term (Eq. 6), in which for clarity of understanding, bottom friction has been dropped, should decrease the local steepness in Eq. 13 by $\left(S^\xi - S_b^\xi\right)$. To reach this effect D_b^ξ must take the following form:

$$D_b^\xi = \rho g h \frac{\partial x^\xi}{\partial x} \left(S^\xi - S_b^\xi\right). \tag{34}$$

On the other hand, at cross-section x^ξ for which the wave breaking does not occur, D_b^ξ equals zero, $D_b^\xi = 0$. The dependence of the parameter D_b^ξ on a critical surface steepness of a wave front S_b^ξ is sketched in Fig. 3.

Figure 4 shows a numerical example of a wave, oncoming from a region of constant water depth, that is running up the slope. In numerical computations its breaking has been hindered. The upper graph shows a wave profile, whereas in the lower graph a local surface steepness, $S = \frac{\partial \zeta}{\partial x}$ is drawn for the same time step of computations. Small disturbances decaying with distance, indicated in the figure with a solid line, are noticeable there. They are only observed for the first wave for which non-smooth connection of *SWL* exists with the wave front (cf.

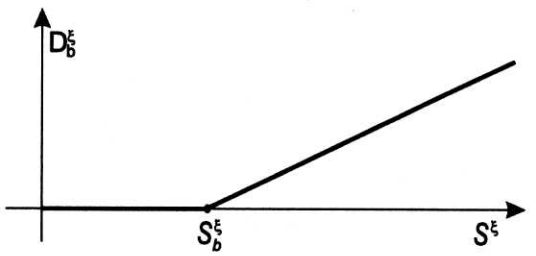

Fig. 3. Influence of critical surface steepness of wave front on momentum loss

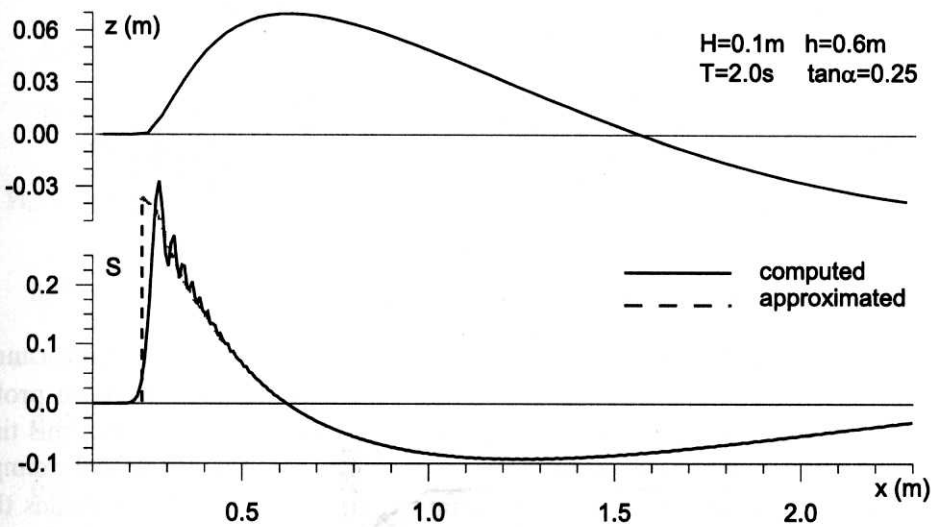

Fig. 4. Profile of wave running up slope (above) and graph of its local surface steepness in case of wave breaking not allowed during numerical computations

upper graph in Fig. 4). The expected plot of the local steepness has been marked in the figure with a dashed line.

Rough information on breaking waves may be assessed from the magnitude of the Iribarren number Ir:

$$Ir = \frac{\tan\alpha}{\sqrt{H/L}}, \tag{35}$$

where α is the angle of a flat beach slope and H/L is the incident wave steepness. A diagram of the Iribarren number has been given in Fig. 5 where separating values of the type of a breaking are taken after Günbak (1977). For the example shown in Fig. 4, the Iribarren number Ir amounts to 1.74. It suggests that a plunging breaker should appear in a laboratory experiment, however in numerical computations the breaking was not simulated. This means that the wave run-up was predicted numerically as for the non-breaking case.

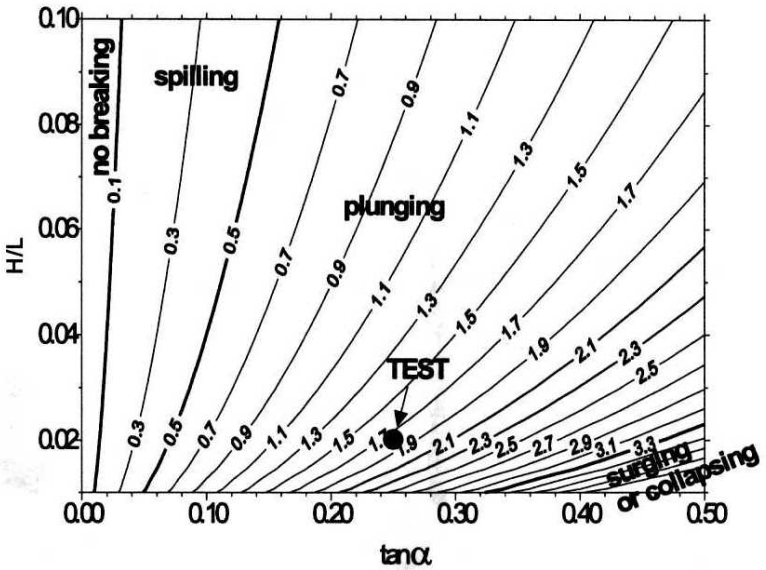

Fig. 5. Diagram of Iribarren number Ir (Kapinski 1998)

As was mentioned earlier, a local steepness of a breaking wave front cannot exceed the critical value of S_b^{ξ} at any point. Figure 6 presents the wave profile with the same initial parameters as in the example shown in Fig. 4, but this time a bore-like breaking process is taken into account. In this computational example S_b^{ξ} was set, by way of example, as a constant value equal to 0.125. It means that the local steepness of a wave front cannot exceed half the inclination of a bottom slope. This has been confirmed by the lower graph in Fig. 6. In this computational example the wave-breaking started at about 1.4 m from the junction of *SWL* with a beach face that corresponds to the origin of co-ordinate system in the model, $x = 0$. Because of the small value of S_b^{ξ}, an exaggerated dissipation rate was imposed there and thus a considerable decay of wave height can be observed. This intentional effect has been shown in Fig. 7, where selected wave profiles for several time steps of computations are drawn.

It should be fairly clear that there exists dependence of a computed wave run-up height R_{up} on the magnitude of the parameter S_b^{ξ}. The confirming example is shown in Fig. 8. For higher values of a permissible local gradient of a wave front S_b^{ξ}, a water tongue achieves a higher position on a slope. Parameter S_b^{ξ} equal to infinity, marked in Fig. 8, denotes the test with a simulation of a non-breaking wave uprush. Finding the magnitude of critical surface steepness, for the case when run-up heights measured in a laboratory and computed numerically are identical, is the goal of the next section.

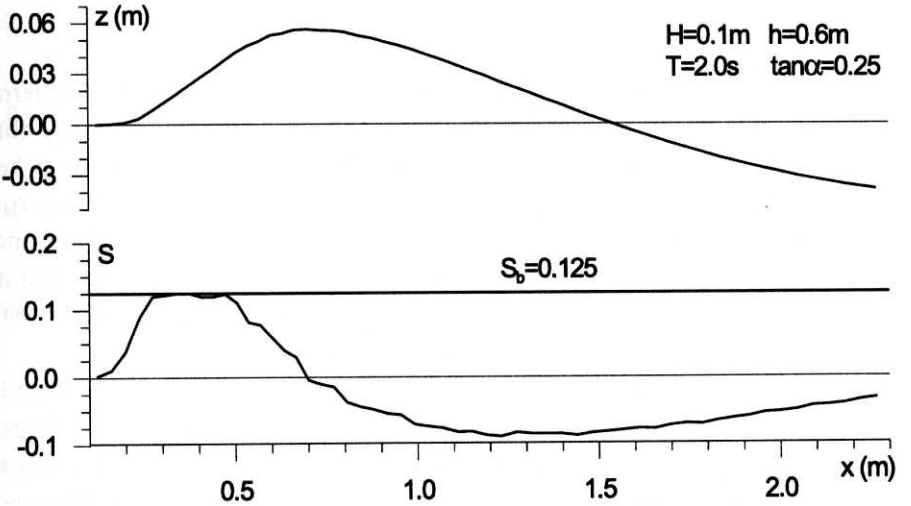

Fig. 6. Profile of breaking wave running up slope and graph of its local surface steepness

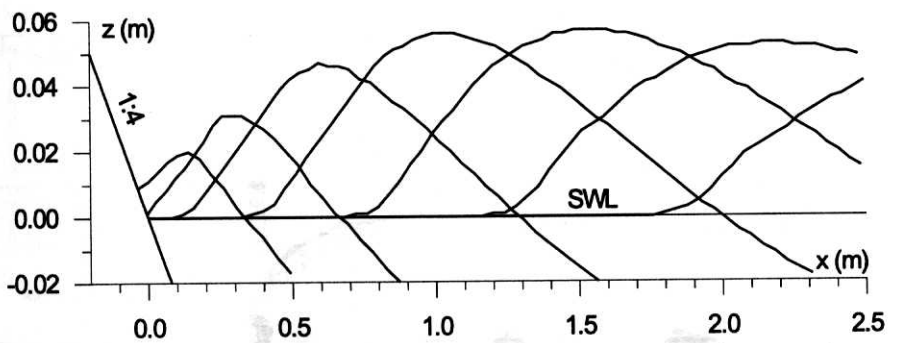

Fig. 7. Run-up of breaking wave on slope for different time steps of computations

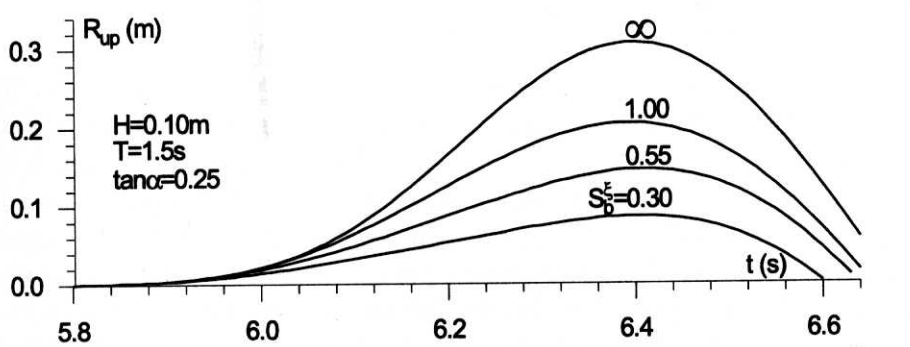

Fig. 8. Breaking wave run-up for different values of critical surface steepness S_b^ξ

5.2. Calibration of S_b^{ξ} Parameter through Experimental Data

In 1992–1995, at the Institute of Hydro-Engineering of the Polish Academy of Sciences (*IH PAS*) in Gdansk, extensive laboratory experiments of a wave run-up phenomenon were performed. The main goal was optimisation of run-up height of irregular waves. These tests concerned several plane slopes and different roughness elements with various localisation on the slopes. General description and selected results of the performed experiments were presented by Kołodko, Kapiński, et al (1996). Some experiments turned out to be helpful in calibration of the presented mathematical model for breaking waves.

A sketch of the *IH PAS* wave flume is shown in Fig. 9. The flume is 20 m long, 0.5 m wide, 1.5 m high and filled in with water in the range of 0.5–0.7 m. To generate waves according to JONSWAP spectrum a piston with wave absorption facilities was used. Water elevations were measured by several fixed capacitance-type gauges, whereas to record uprush-backwash excursions, two wires located on the slope 5 mm over its surface were installed.

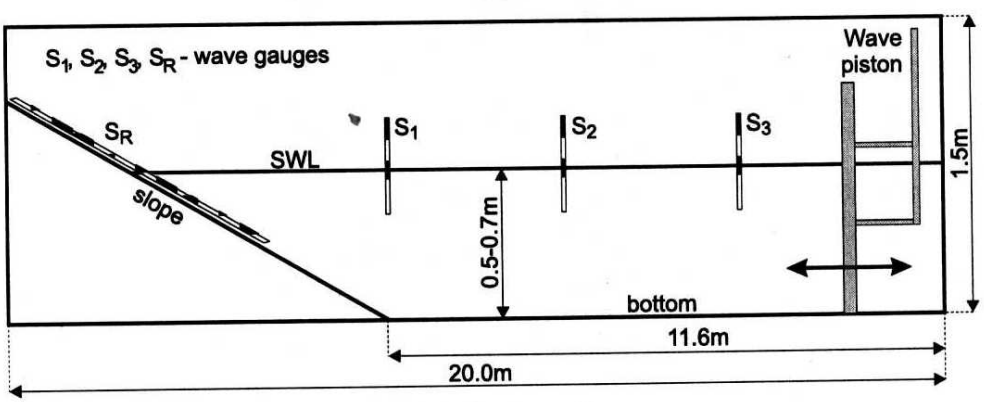

Fig. 9. Sketch of wave flume

The aim of the calibration was to obtain the magnitude of the critical steepness S_b^{ξ} for the case when measured and computed run-up heights are identical. The result of this work is shown in Fig. 10. Runs of regular waves are marked with solid triangles, whereas those of irregular ones – with solid circles. Next to each experiment the proper values of the computed parameter S_b^{ξ} are given. The laboratory experiments were carried out for a smooth slope made of plywood, therefore the influence of bottom friction can be neglected. Inclination of the slope was the same for each experiment: $\tan\alpha = 0.25$, whereas the Iribarren number Ir was approximately in the range of 1.2–2.0. The significant wave run-up height R_{us} was calculated as an average height of one-third of the highest run-ups. These experiments have shown that there is little difference in extreme values of

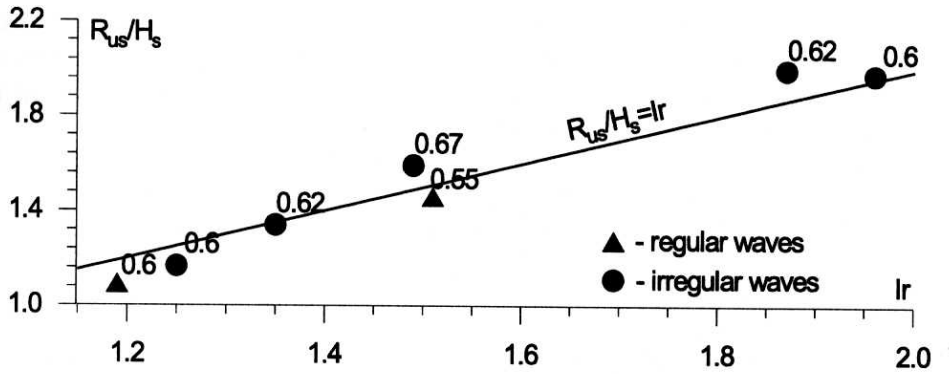

Fig. 10. Calibration of critical steepness parameter S_b^{ξ}

the parameter S_b^{ξ}. Its mean value is equal to 0.61 and corresponds to the maximum angle of a wave front of 31°. It means that for the slope inclination 1 : 4 measured and computed run-up heights of breaking waves are almost identical when the parameter of a critical steepness of a wave front is equal to 0.61.

A rough comparison of many other numerical tests (not presented here) with the Hunt formula (Hunt 1959):

$$\frac{R_{up}}{H} = \frac{\tan\alpha}{\sqrt{H/L}}, \tag{36}$$

suggests that there exists only slight dependence of the parameter S_b^{ξ} on a slope angle α and that it seems to be the only factor. Hence, taking this into account, the following condition can been postulated:

$$S_b^{\xi} = \psi \tan\alpha, \tag{37}$$

where ψ is a constant or function with gentle progress.

6. Discussion on Numerical Modelling of Flow and Orbital Velocities

As is well known, non-breaking sinusoidal waves approaching a shore show sinusoidal swash oscillations on a uniformly inclined slope. This was pointed out by e.g. Miche (1944), Kemp and Plinston (1974) and Horikawa (1988). Maximum velocity appears at the point of junction of the mean water level with the slope ($x = 0$ in Fig. 1), although the maximum acceleration a water tongue tip has in the extreme waterline positions. It has been tested and confirmed here by numerical simulations. An example of a horizontal displacement, velocity and acceleration of the moving shoreline is given in Fig. 11. Oncoming regular waves ($H = 0.1$ m, $T = 3$ s) from a region with a constant depth, $h = 0.6$ m, are analysed. They run the uniform slope with an inclination of 1 : 1 up. All parameters presented in the figure are described by a time-dependent sinusoidal function. For the same

numerical experiment a water surface elevation, as well as horizontal flow velocity and acceleration at the cross-section $x = 0$ have been examined. The results are shown in Fig. 12. They only cover the period while the water body exists in the cross-section, i.e. $t = T/2$.

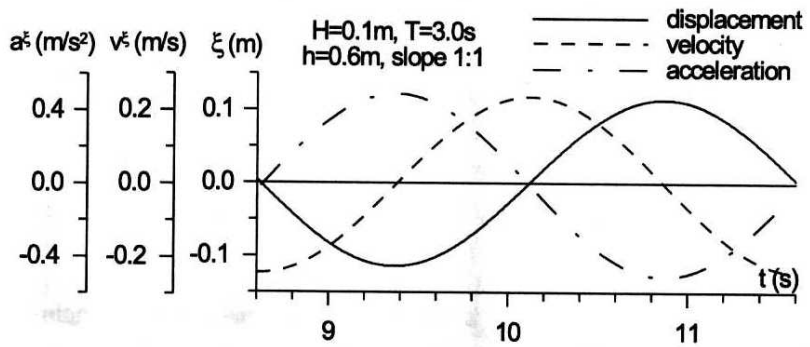

Fig. 11. Horizontal displacement, velocity and acceleration of floating tongue tip

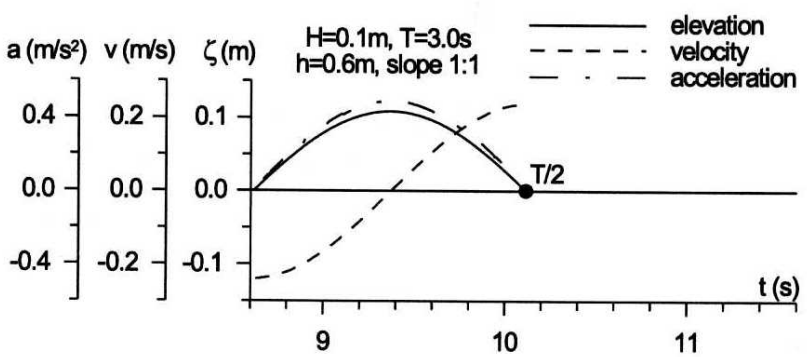

Fig. 12. Water elevation, horizontal velocity and acceleration at connection of *SWL* with slope

As has been shown earlier, the model is capable of computing mass transport. Despite the reverse direction, it has the same magnitude of velocity as a return flow computed in this model. The most simple numerical example is given in Fig. 13 where a long wave ($H = 0.1$ m, $T = 3$ s) travels in a channel with constant depth, h=0.6 m. The upper graph concerns a progressive wave, whereas in the lower graph the results for a standing wave are shown. A dashed line in the upper graph describes the particle velocity during a single wave period T. Computed time-averaged particle velocity is equal to zero, $\overline{v^{\xi}} = 0$ (also cf. Eq. 22). The solid line, when compared with the sinusoidal graph of the particle velocity, has a flatter crest in the second quarter and steeper trough in the third. Therefore the time-averaged flow velocity has a non-zeroth offshore direction. Computed numerically, the magnitude of the return flow amounts here to 0.084 m/s. The

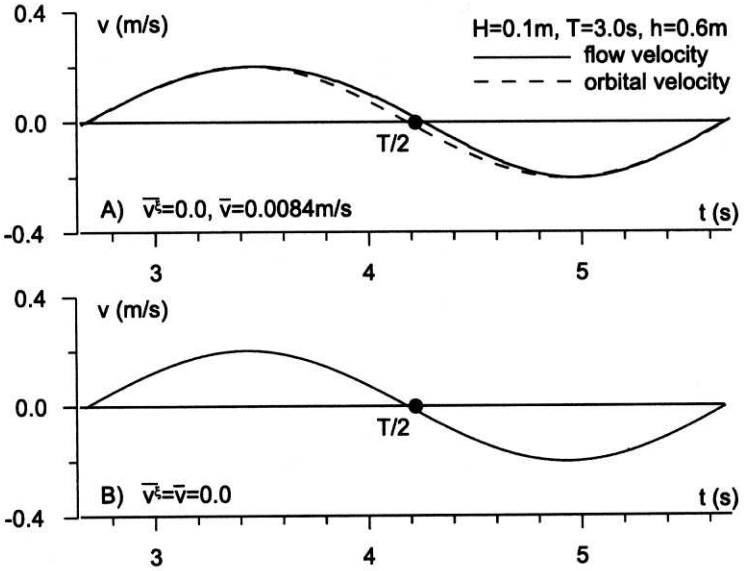

Fig. 13. Depth-averaged particle and return flow velocity at constant depth for progressive (A) and standing (B) wave

lower graph in Fig. 13 shows velocities for the standing wave. The dashed line is invisible, as it is overlapped by the solid one. Mean values of both velocities computed for this case are equal to zero. This means that for standing waves a mass transport does not exist in the model.

Figure 14 shows another example of return flow modelling. An initially regular wave (H = 0.2 m, T = 3 s) advances over a decreasing bottom depth, h = 1.0–0.6 m. Computed values of a return flow have been marked by solid circles and next connected with straight solid lines. As is shown the velocity of a return flow (and mass transport velocity corresponding to it) has a tendency to grow as the water depth becomes smaller.

Figure 15 shows an example of the spatial distribution of a velocity in the swash zone and its offshore vicinity. A sketch of the numerical channel with marked computed wave profiles in two extreme positions on the slope is also given. The solid circles indicate computed maximum and mean velocities at selected cross-sections. Extreme positive and negative velocities are symmetrical to each other, while the mean motion is equal to zero in the whole area of computations. At x = 0 the flow velocity is maximal and rapid decrease in the landward direction is observed.

In Fig. 16 a similar example of velocity distribution as in Fig. 15 is presented, but this time it is shown that the maximum velocity at the beach face in some cases can be smaller than the maximum velocity in the neighbouring offshore vicinity.

Figure 17 shows comparison of numerical simulations with the Miche (1944) analytical solution (Eq. 1). Some discrepancy appears here, although in both cases

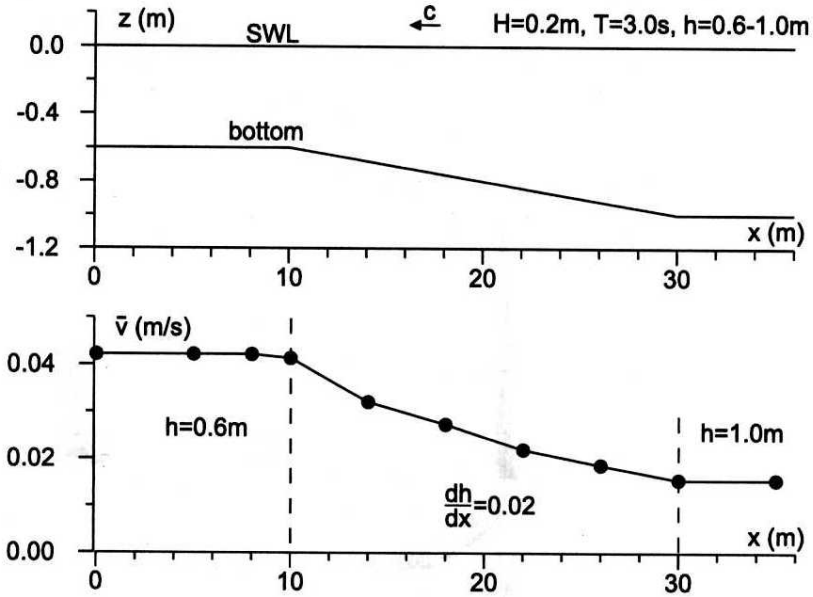

Fig. 14. Time-averaged return flow over varying water depths (black circles – computations)

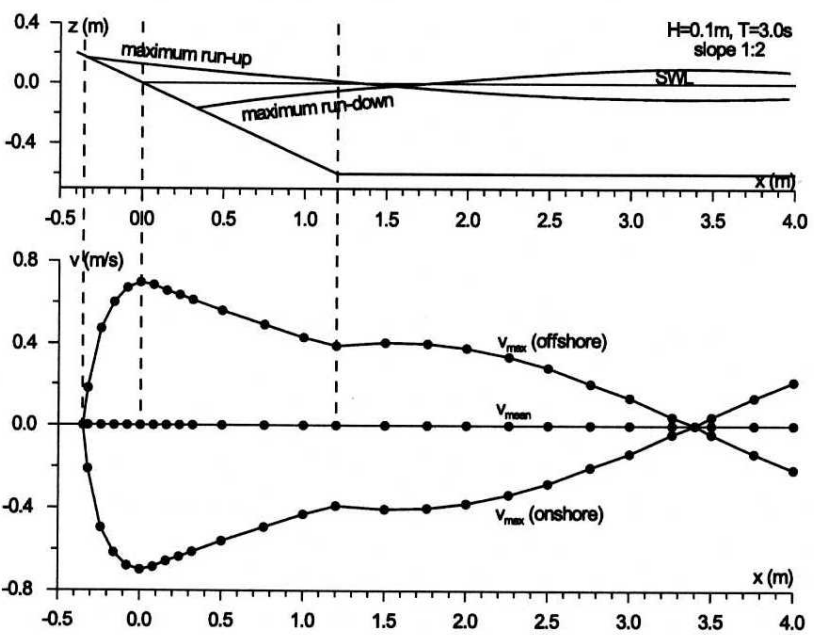

Fig. 15. Example of extreme and mean flow velocities for standing wave run-up (black circles – computations)

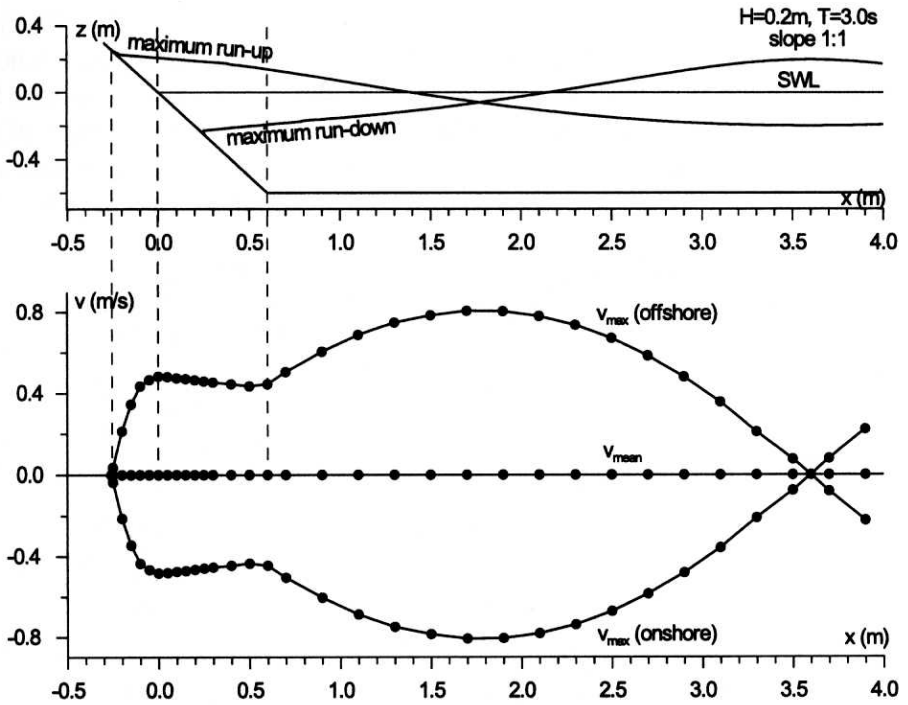

Fig. 16. Another example of extreme and mean flow velocities for standing wave run-up (black circles – computations)

dependence $v_{0\,max} \sim 1/\sqrt{L}$ can be observed. The reason for this diversity has not been found.

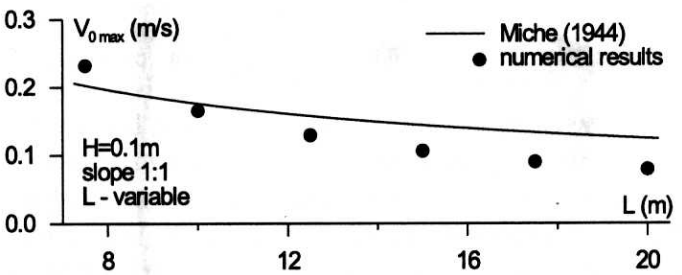

Fig. 17. Comparison of numerical computations with Miche solution (1944)

When a wave breaking phenomenon does not occur, bottom friction seems to be an important factor in flow velocity and run-up height attenuation. In the present model two crude formulas based on depth averaged velocities are used (Eqs. 31, 32). The aim of numerical analysis was not an assessment of a magnitude of coefficients but rather the effect of adopted formulas on the shoreward wave transformation. For better visualisation much more exaggerated dissipation has been taken in computations (i.e. large friction coefficients). In Fig. 18 are

presented results of attenuation both by linear friction (Voltzinger et al 1989) and quadratic friction formula. The upper graph shows water surface profiles, whereas in the lower graph flow velocities are given. Magnitudes of friction factors have been chosen suitably to demonstrate that it does not matter what kind of friction formula is used in the model. Both of them give approximately the same attenuation of wave height and flow velocity along the numerical channel.

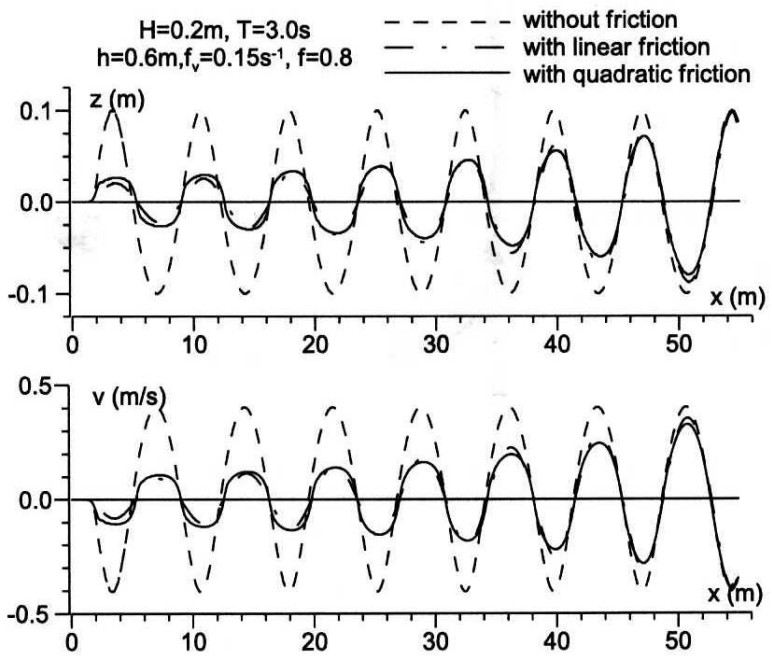

Fig. 18. Wave profile and flow velocity in case of bottom friction

Sea or ocean waves approaching a shore very often break on a natural beach or on man-made slopes. Knowledge of spatial velocity distribution in the swash zone is then important both for modelling of sediment transport and forecasting of damage conditions of breakwaters or mounds. The upper graph in Fig. 19 shows horizontal displacement of a water tongue tip during simulation of a wave breaking in the model. With the solid line the tip elevation has also been marked. In the middle graph flow and particle velocities are drawn. The solid line indicates the velocity of the tongue tip on the slope, whereas the dashed line represents the flow velocity at the junction of *SWL* with the beach ($x = 0$ in Fig. 1). Contrary to a non-breaking wave run-up (cf. Fig. 15 and 16), maximum velocity appears somewhere between run-on length R_{on} and the junction of *SWL* with the beach, $x = 0$. The lower graph in Fig. 19 shows the distribution of a water tongue acceleration during the uprush-backwash period. All these graphs, contrary to standing wave run-up, are not sinusoidal functions. Moreover, it can be

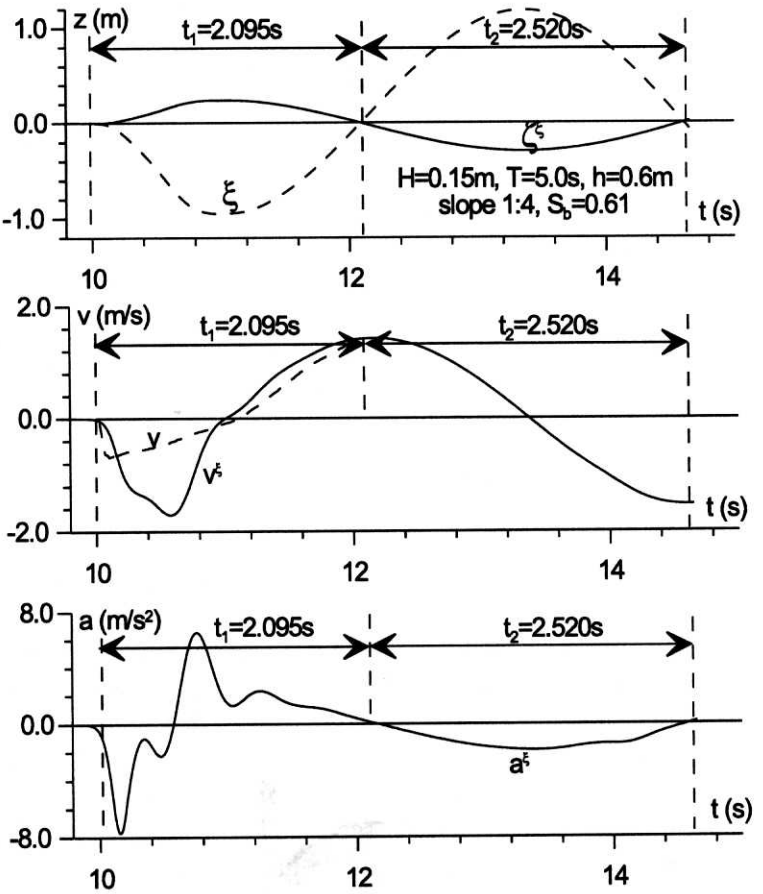

Fig. 19. Displacements, velocities and acceleration in case of breaking wave run-up

observed that for the breaking wave, run-up period is shorter than the run-down period. For this numerical example, when bore-like breaking wave runs the slope up, particle trajectories are also computed and shown in Fig. 20. For better visualisation parameter S_b^{ξ} has been decreased about 2.5 times, i.e. stronger condition due to wave breaking has been imposed. The solid circles in the figure indicate initial positions of the particles.

In Figure 21 a spatial distribution of flow velocities caused by a single breaking wave is given. The upper graph shows a shot of a bore profile during the run-up phase, whereas in the middle graph, computed maximum and mean velocities are marked. They are the complex effect of interaction of a wave-breaking phenomenon on swash oscillations. Contrary to the standing wave (cf. Fig. 15 and 16), the maximum landward and seaward velocities are not symmetrical to each other. Additionally, the maximum shoreward velocity is bigger than the maximum seaward velocity and it does not perform at the junction of *SWL* with the slope but somewhere inside the run-up region. Moreover, the mean flow velocity is

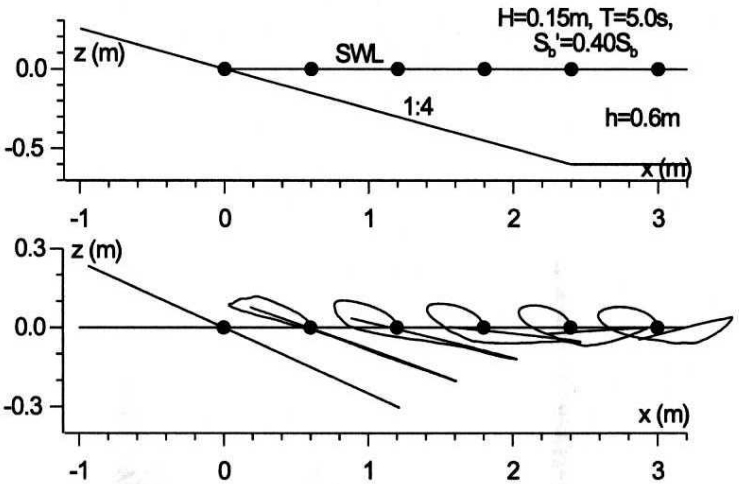

Fig. 20. Particle trajectories of breaking wave in swash zone and its offshore vicinity

not zeroth along the analysed area. On the right-hand side of the cross-section B–B, a small offshore mean current is observed, while in the opposite region a current, exists, but seems to be negligibly small. The computed incipience of a wave breaking is located near cross-section A–A in Fig. 21, and thus the decrease in magnitude of the mean velocity is observed there. It is worth mentioning that in numerical computations the time-averaging outside the swash zone was made over a wave period, whereas inside the swash zone it concerned a period of the presence of a water body at a given cross-section. The lower graph in Fig. 21 shows a velocity distribution presented in the middle graph that has been normalised by a local wave celerity $c = \sqrt{gh}$.

7. Summary

A simple mathematical model for prediction of shallow-water wave propagation has been presented. The model was applied to simulation of wave and water motion in the swash zone and its seaward vicinity. Such phenomena as wave run-up, water flow and orbital motion have been discussed. Waves influenced by bottom friction were modelled using formulas that are linear or quadratic with an orbital velocity. The wave breaking was simulated as an analogy to bore propagation where as a breaking criterion a limited local slope of a wave front was taken. The model for breaking waves has been calibrated for plane impermeable slopes with an inclination 1 : 4. Selected results of numerical computations were presented in graphical form and for simplified cases some analytical results were derived. Although the examples presented are shown for simple bathymetric profiles, the model can also be used for prediction of a wave and water motion over more complex bottoms.

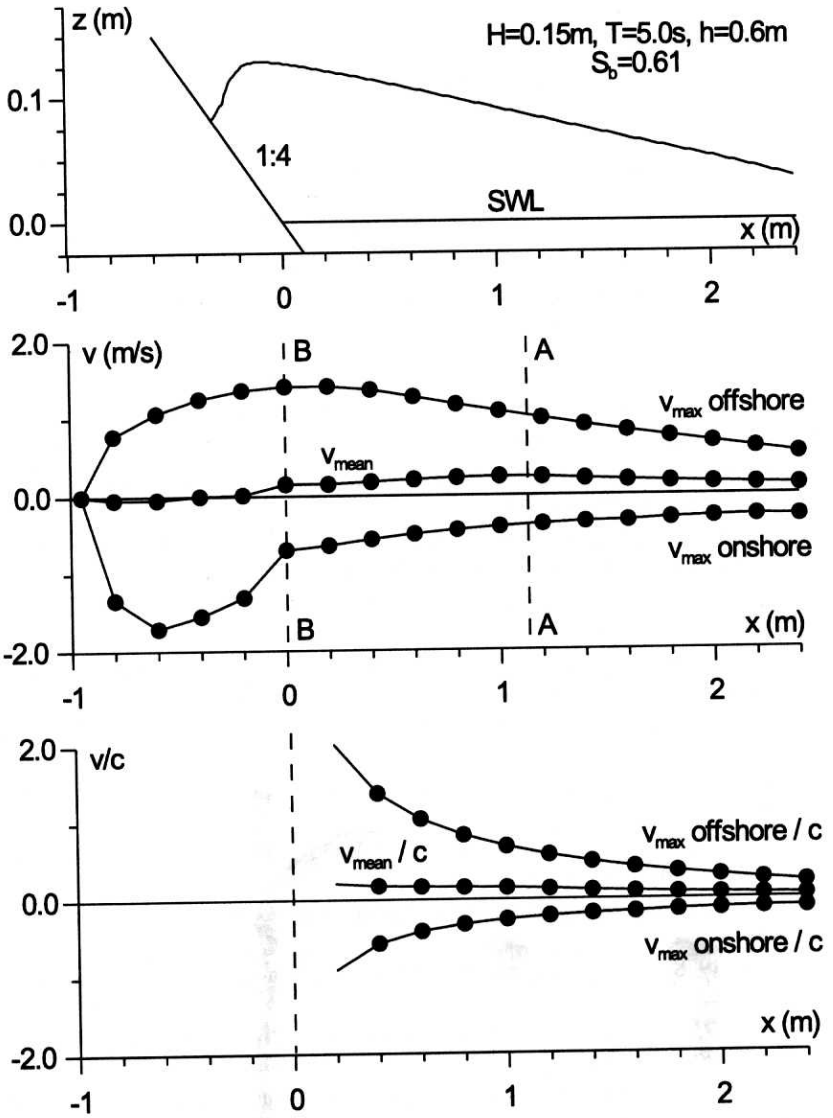

Fig. 21. Example of extreme and mean flow velocities for breaking wave run-up

References

Andrews D. G., McIntyre M. E. (1978), An Exact Theory of Nonlinear Waves on a Lagrangian-mean Flow, *Jour. Fluid Mech.*, Vol. 89, Part 4, 609–646.

Dingemans M. W. (1997), Water Wave Propagation over Uneven Bottoms. Part 1 – Linear Wave Propagation, *Advanced Series on Ocean Engineering*, Vol. 13, World Scientific Publ. Co., 227–243.

Goto Ch. (1979), Nonlinear Equation of Long Waves in the Lagrangian Description, Coastal Engineering in Japan, Vol. 22, 1–9.

Günbak A. R. (1977), *Rubble Mound Breakwaters*, Div. Port and Ocean Engineering, Rep. No. 12/77, Technical University of Norway, Trondheim.

Horikawa K. (editor) (1988), *Nearshore Dynamics and Coastal Processes. Theory, Measurements and Predictive Models*, University of Tokyo Press.

Hunt I. A. (1959), Design of Seawalls and Breakwaters, *Proceedings of ASCE, Journal of Waterways and Harbors Division*, Vol. 85, 123–152.

Iribarres R., Nogales C. (1949), Protection des ports, *XVII International Navigation Congress*, Lisbon, SII-4.

Kapiński J. (1998), *A Hybrid Model of Wave Propagation and Wave Run-up on Slope*, Ph.D. Thesis, Institute of Hydro-Engineering, Polish Academy of Sciences, Gdansk, 159 pp. (in Polish).

Kapiński J., Kołodko J. (1996), Wave Run-up on Gentle Slopes: a Hybrid Approach, *Archives of Hydro-Engineering and Environmental Mechanics*, IH PAS Gdansk, Vol. 43, No. 1–4, 79–89.

Keller J. B., Keller H. B. (1964), *Water Wave Run-up on a Beach*, Research Report No. NONR 3828(00), Office of Naval Research, Department of the Navy, Washington D.C., New York.

Kemp P. H., Plinston D.T. (1974), Internal Velocities in the Uprush and Backwash Zone, *Coastal Engineering*, Chapter 32, 575–585.

Kołodko J., Kapiński J., Szmytkiewicz M., Zeidler R. B. (1996), Wave Run-up: Recent IBW PAN Investigations, *Coastal Dynamics '95*, ASCE, New York, 197–208.

McIntyre M. E. (1980), Towards a Lagrangian-mean Description of Stratospheric Circulations and Chemical Transports, Phil. Trans. Roy. Soc., London, A296, 129–148.

Miche A. (1944), Mouvements Ondulatoires de la Mer en Profondeur Constante ou Décroissante, *Annales des Ponts et Chaussées*.

Nishimura H., Takewaka S. (1987), Numerical Analysis of Surface Waves using Lagrangian Description, *Coastal Engineering in Japan*, Vol. 30, No. 1, 1–7.

Shuto N. (1967), Run-up of Long Waves on a Sloping Beach, *Coastal Engineering in Japan*, Vol. 10. 23–38.

Shuto N. (1968), Three Dimensional Behaviour of Long Waves on a Sloping Beach, *Coastal Engineering in Japan*, Vol. 11, 53–57.

Shuto N. (1972), Standing Waves in Front of a Sloping Dike, *Coastal Engineering in Japan*, Vol. 15, 13–23.

Shuto N., Goto T. (1978), Numerical Simulation of Tsunami Run-up, *Coastal Engineering in Japan*, Vol. 21, 13–20.

Van Rijn L. C. (1993), *Principles of Sediment Transport in Rivers, Estuaries and Coastal Seas*, Aqua Publications, Netherlands.

Voltzinger N. E., Klevanny K. A., Pelinovsky E. N. (1989), *Long-wave Dynamics of the Coastal Zone*, Gidrometeoizdat Publishers, Leningrad (in Russian).

Von Neumann J., Richtmyer R. D. (1950), A Method for the Numerical Calculation of Hydrodynamic Shocks, *Jour. Appl. Phys.*, 21, 232–237.

Zelt J. A. (1991), The Run-up of Nonbreaking and Breaking Solitary Waves, *Coastal Engineering*, 15: 205–246.

Zelt J. A., Raichlen F. (1990), A Lagrangian Model for Wave Induced Harbour Oscillations, *Jour. Fluid Mech.*, 213: 203–228.